Surface tension of an electrolyte–air interface: a Monte Carlo study

2012 J. Phys.: Condens. Matter 24 284115

(http://iopscience.iop.org/0953-8984/24/28/284115)

J. Phys.: Condens. Matter **24** (2012) 284115 (5pp) doi:10.1088/0953-8984/24/28/284115

Surface tension of an electrolyte–air interface: a Monte Carlo study

Alexandre Diehl[1], **Alexandre P dos Santos**[2] **and Yan Levin**[2]

[1] Departamento de Física, Instituto de Física e Matemática, Universidade Federal de Pelotas, Caixa Postal 354, CEP 96010-900, Pelotas, RS, Brazil
[2] Instituto de Física, Universidade Federal do Rio Grande do Sul, Caixa Postal 15051, CEP 91501-970, Porto Alegre, RS, Brazil

E-mail: levin@if.ufrgs.br

Received 27 September 2011
Published 27 June 2012
Online at stacks.iop.org/JPhysCM/24/284115

Abstract
We present a new method for calculating the surface tension of an electrolyte–air interface using Monte Carlo (MC) simulations with an implicit solvent in a spherical drop geometry. The boundary conditions for the electric field at the interface are accounted for using image and counter-image charges. The density profiles obtained from the simulations are used to calculate the excess surface tension of the electrolyte–air interface using the Gibbs adsorption isotherm equation. The results are found to be in good agreement with experiments and the earlier theoretical calculations.

(Some figures may appear in colour only in the online journal)

1. Introduction

Electrolyte solutions have been a subject of intense study for over 100 years. While the bulk thermodynamics of electrolytes is reasonably well understood [1, 2], this is not the case for their surface properties. In spite of a significant effort to account for ion–surface interactions both theoretical [3–11] and experimental [12–14], a complete understanding is still lacking. The electrolyte–air interface, for instance, remains a fascinating topic of discussion since Heydweiller's experimental measurements of surface tensions of salts dissolved in water [15]. Heydweiller noticed that the surface tension of the electrolyte–air interface depends specifically on the ions present in solution. Curiously the effect of different electrolytes on the surface tension of water observed by Heydweiller mimicked closely their influence on the stability of protein solutions discovered by Hofmeister 20 years earlier [16]. The two effects seem to be intimately connected, but the relationship between them is not very clear.

The interface between an electrolyte and a protein or between an electrolyte and a hydrophobic surface is of paramount importance in many biological applications. In addition, much of the atmospheric chemistry, and in particular the rate of ozone depletion, depends strongly on the presence of ions at the surface of aerosol particles [17]. Recent work suggests that ions at the air–water interface or near a hydrophobic surface can be divided into two classes: the kosmotropes and the chaotropes [10]. Kosmotropes remain hydrated and are repelled from the interface, while the chaotropes lose their hydration sheath and, as a consequence of their large polarizability, become adsorbed at the air–water interfaces or at a hydrophobic surface [18]. These conclusions were obtained using a modified Poisson–Boltzmann equation, which neglects the electrostatic and hard-core correlations between the ions. In the present work we would like to quantitatively check the predictions of the Poisson–Boltzmann theory against the Monte Carlo simulations.

2. Model system and Monte Carlo methodology

2.1. Model system

We study a primitive model of a monovalent electrolyte confined to a spherical mesoscopic drop of water of radius R, corresponding to the position of the Gibbs dividing surface (GDS) [19]. The drop contains N pairs of cations and anions with radii r_c and r_a, respectively. Water and air are treated as uniform dielectric media of permittivities $\epsilon_w = 80$ and $\epsilon_a = 1$,

respectively. The system is at room temperature, so that the Bjerrum length is $\lambda_B = q^2/\epsilon_w k_B T = 7.2$ Å. The dielectric discontinuity at the air–water interface results in an induced surface charge. For a planar geometry this is a well-known problem, the solution of which goes back to Lord Kelvin [20]. For curved surfaces, on the other hand, it is difficult to properly account for the boundary conditions on the electric field imposed by the Maxwell equations, and numerical calculations must be used [21]. For spherical geometry, however, it is possible to satisfy the required boundary conditions using a combination of image and counter-image charges [22, 23]. Recently this approach was used to study polarizable colloids and nanoparticles, which in general have a dielectric constant much lower than that of water [24, 25]. In that case an ion of a colloidal suspension induces an image and a counter-image charge inside a spherical colloidal particle. The image charge is located at the inversion point, while a continuous distribution of counter-image line charge extends from the center of the colloidal particle to the inversion point. This construction allows one to precisely satisfy the boundary conditions imposed by the Maxwell equations at the dielectric interface [22, 23].

For the present problem, on the other hand, an ion of charge q_i is located inside the spherical water drop and its image and counter-image charges are outside the drop. The situation is the opposite of the colloidal suspension for which ions were located outside the low dielectric sphere. Nevertheless, it is still possible to construct a combination of image and counter-image charges which will allow us to precisely satisfy the boundary conditions at the air–water interface [22, 23]. If the ion is located at position $\mathbf{r}_i$ the image charge of magnitude $q_i' = \gamma q_i R/r_i$ will be located at $\mathbf{r}_i' = (R^2/r_i^2)\mathbf{r}_i$, where $\gamma = (\epsilon_w - \epsilon_a)/(\epsilon_w + \epsilon_a)$. However, this is not sufficient to satisfy the boundary conditions on the electric field. It is also necessary to place a counter-image charge of line density

$$\lambda(u) = \frac{q_i}{R}\frac{\gamma(1+\gamma)}{2}\left(\frac{u}{r_i'}\right)^{-(1-\gamma)/2}, \qquad (1)$$

extending from the position of the image charge to infinity along the radial direction [22, 23], see figure 1. The electrostatic potential produced by the image charge at an arbitrary position $\mathbf{r}$ inside the drop is given by

$$\psi_{im}(\mathbf{r};\mathbf{r}_i) = \frac{q_i'}{\epsilon_w|\mathbf{r} - \frac{R^2}{r_i^2}\mathbf{r}_i|}, \qquad (2)$$

while the electrostatic potential produced by the counter-image line charge is

$$\psi_{ci}(\mathbf{r};\mathbf{r}_i) = \frac{R^2}{\epsilon_w r_i}\int_1^\infty d\eta \frac{\lambda\left(\eta\frac{R^2}{r_i}\right)}{|\mathbf{r} - \eta\frac{R^2}{r_i^2}\mathbf{r}_i|}. \qquad (3)$$

Since for the air–water interface $\epsilon_w \gg \epsilon_a$, the line-charge density can be taken to be uniform, $\lambda(u) = q_i/R$. The integral in equation (3) can then be performed analytically, yielding

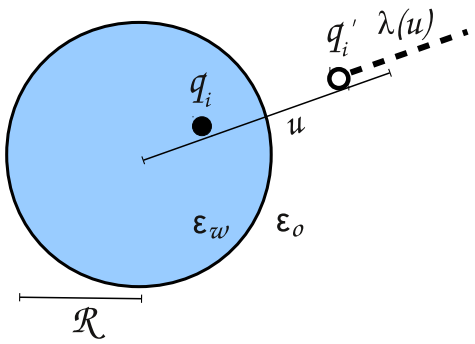

Figure 1. An illustrative representation of an ion of charge q_i, located at $\mathbf{r}_i$ inside a water drop, and its image charge q_i', located at the inversion point $\mathbf{r}_i'$. The counter-image charge $\lambda(u)$ is distributed from the inversion point to infinity.

the counter-image potential at an arbitrary position $\mathbf{r}$:

$$\psi_{ci}(\mathbf{r};\mathbf{r}_i) = -\frac{q_i}{\epsilon_w R} \times \log\left(\frac{R^2 - \mathbf{r}\cdot\mathbf{r}_i + \sqrt{R^4 - 2R^2\mathbf{r}\cdot\mathbf{r}_i + r^2 r_i^2}}{2R^2}\right). \qquad (4)$$

The ion–counter-image interaction potential (for $\mathbf{r} = \mathbf{r}_i$) reduces to

$$\psi_{ci}^{self}(\mathbf{r}_i) = -\frac{q_i}{\epsilon_w R}\log\left(1 - \frac{r_i^2}{R^2}\right). \qquad (5)$$

Using the expressions above, the electrostatic potential produced at position $\mathbf{r}$ by a charge q_i located at $\mathbf{r}_i$ is given by

$$\phi(\mathbf{r};\mathbf{r}_i) = \frac{q_i}{\epsilon_w|\mathbf{r} - \mathbf{r}_i|} + \frac{q_i R}{\epsilon_w r_i|\mathbf{r} - \frac{R^2}{r_i^2}\mathbf{r}_i|} + \psi_{ci}(\mathbf{r};\mathbf{r}_i), \qquad (6)$$

where the first term is the electrostatic potential of the ion, the second term is the potential of the image charge and the last term is the potential produced by the counter-image charge. The work required to bring all the ions from infinity to their respective positions inside the drop is

$$U = \sum_{i=1}^{N-1}\sum_{j=i+1}^{N} q_j\phi(\mathbf{r}_j;\mathbf{r}_i) + \sum_{i=1}^{N}\frac{q_i^2 R}{2\epsilon_w(R^2 - r_i^2)} + \frac{1}{2}\sum_{i=1}^{N} q_i\psi_{ci}^{self}(\mathbf{r}_i), \qquad (7)$$

where the last two terms are the self-interaction energy of the ion with its own image and counter-image charges, respectively.

2.2. Monte Carlo simulation inside the drop

We have used canonical Monte Carlo (MC) simulations in order to obtain the density profiles of cations and anions inside the water drop. Two types of MC moves were used—for low electrolyte concentration, ion transfer to a completely new random position inside the drop, and for higher concentrations

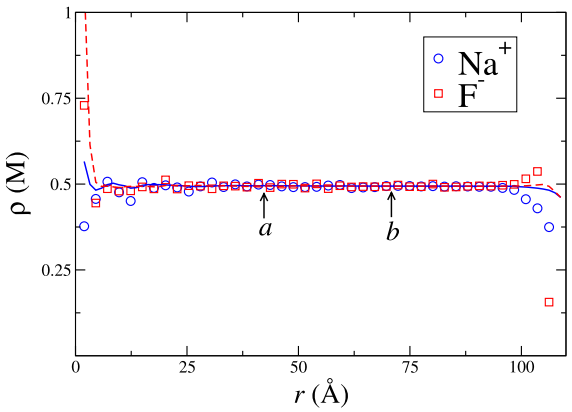

Figure 2. Density profiles for NaF at 0.5 M concentration. The solid and dashed lines represent the auxiliary functions $f_{\pm}(r)$ for Na^+ and F^-, respectively, used to obtain the bulk concentration, c_b, at the center of the drop. The points a and b are the limits used in equation (9) to obtain c_b. The drop radius is $R = 110$ Å.

a small linear displacement in order to give the standard acceptance ratios for the Metropolis algorithm [26]. Typical runs involved equilibration and production, each of 10^5 steps per particle. After equilibration, uncorrelated states were generated at intervals of ten steps per particle, creating a total of 10^4 uncorrelated configurations. After equilibration, the average number of cations and anions in concentric spherical shells of equal thickness were accumulated in order to obtain the ionic density profiles, $\rho_{\pm}(r)$, where r is the distance from the center of the drop. In figure 2 we show typical density profiles for NaF.

The accuracy of the ionic density profiles near the center of the drop is affected by the geometry of the system—since the bins close to the origin have only a few particles, they are strongly susceptible to thermodynamic fluctuations, see figure 2. To obtain an accurate estimate of the bulk concentration of the electrolyte, $c_b = \rho_+(0) = \rho_-(0)$, we introduce auxiliary functions, $f_{\pm}(r)$, which give us smoothed-out density profiles in the central region of the drop:

$$f_{\pm}(r) = \frac{3}{r^3}\int_0^r \mathrm{d}r'\; r'^2 \rho_{\pm}(r'). \tag{8}$$

The bulk concentration of the salt is then calculated as an average of the coarse-grained densities of cations and anions $f_{\pm}$ between the two radial positions, a and b, in the flat region indicated in figure 2:

$$c_b = \frac{1}{b-a}\int_a^b \mathrm{d}r' \frac{f_+(r') + f_-(r')}{2}. \tag{9}$$

To calculate the excess surface tension γ we integrate the Gibbs adsorption isotherm equation, $\mathrm{d}\gamma = -\Gamma_+ \mathrm{d}\mu_+ - \Gamma_- \mathrm{d}\mu_-$, where $\mu_{\pm}$ are the chemical potentials of cations and anions, respectively, and $\Gamma_{\pm}$ are the ion excess per unit area defined as

$$\Gamma_{\pm} = \frac{1}{4\pi R^2}\left[\int_0^{\infty} \rho_{\pm}(r) 4\pi r^2\, \mathrm{d}r - \frac{4\pi R^3}{3} c_b\right]. \tag{10}$$

If the water drop contains N pairs of cations and anions, equation (10) simplifies to $\Gamma_{\pm} = N/4\pi R^2 - c_b R/3$, where c_b is given by equation (9). Due to spherical symmetry and charge neutrality, the Gibbs adsorption isotherm equation can also be written as $\mathrm{d}\gamma = -\Gamma\, \mathrm{d}\mu$, where $\Gamma = \Gamma_+ = \Gamma_-$ and $\mu = \mu_+ + \mu_-$ is the salt chemical potential.

2.3. Grand-canonical simulation

To obtain the chemical potential for a given bulk concentration of electrolyte c_b, we use grand-canonical Monte Carlo (GCMC) simulations. In such simulations, the system—a cubic box of length L, with periodic boundary conditions—is placed in contact with a salt reservoir at chemical potential μ. We start with a trial $2N$ ions, half carrying a charge $+q$ and the other half a charge $-q$. The diameters of cations and anions are $\sigma_+ = 2r_c$ and $\sigma_- = 2r_a$, respectively. The interaction potential between two non-overlapping charges separated by a distance r_{ij} is $U_{ij} = q_i q_j/\epsilon_w r_{ij}$. To maintain the electroneutrality of the system, we have used unbiased ion pair additions and removals at each time step, with a standard grand-canonical MC algorithm. The simulations were performed using the discretization methodology introduced by Panagiotopoulos and Kumar [27], where the allowed positions for the ion centers are restricted to a simple cubic grid of spacing l. Hence, the discretization parameter is defined as $\zeta = \sigma_{\pm}/l$, where $\sigma_{\pm} = (\sigma_+ + \sigma_-)/2$ is the unlike-ion collision diameter. We have used in our simulations $\zeta = 10$, which reproduces essentially the same results of the continuum model [27], with a significant economy in simulation time. The long-range Coulomb interactions are calculated with the Ewald summation method employing conducting boundary conditions and using 518 Fourier-space wavevectors and real-space damping parameter $\kappa = 5/L$.

The reduced temperature and electrolyte concentrations are defined as

$$T^{\star} = k_B T \epsilon_w \sigma_{\pm}/q^2 \qquad \text{and} \qquad \rho^{\star} = N\sigma_{\pm}^3/L^3, \tag{11}$$

while the reduced salt chemical potential is $\mu^{\star} = \mu \epsilon_w \sigma_{\pm}/q^2$, so that in the limit of high temperatures and low densities we obtain

$$\mu^{\star} \to 2T^{\star} \ln \rho^{*}. \tag{12}$$

Note that the reduced temperature and chemical potential can also be written as $T^{\star} = \sigma_{\pm}/\lambda_B$ and $\mu^{\star} = (\sigma_{\pm}/\lambda_B)\mu/k_B T$, respectively. In figure 3 we show the reduced salt concentration as a function of the chemical potential μ used in GCMC simulations. Figure 3 can then be used to construct $\mu(c_b)$. Inserting this expression into the Gibbs adsorption isotherm and integrating numerically, we obtain the excess surface tension for the electrolyte–air interface.

3. Results and discussion

First, we study the alkali metal chloride salts. We begin with NaCl. In our earlier work based on the modified Poisson–Boltzmann equation, it was found that Cl^- is on the borderline between the kosmotropes (structure-making) and chaotropes (structure-breaking ions) [9, 10]. Specifically,

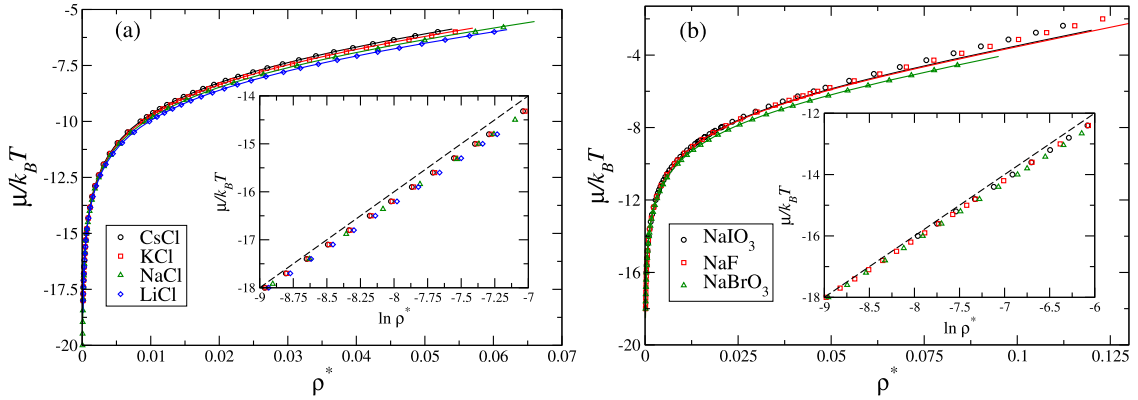

Figure 3. The chemical potential of salt μ, as a function of reduced salt concentration obtained using the GCMC simulations for (a) alkali metal chloride salts and (b) sodium fluoride, iodate and bromate salts. The Bjerrum length is $\lambda_B = 7.2$ Å. Solid lines are the chemical potentials obtained using the mean spherical approximation (MSA) [19]. The insets show the ideal gas limit (dashed line), equation (12).

it was found that Cl^- remains weakly hydrated at the air–water interface, with a hydration radius very close to its crystallographic one, 2 Å. To fit the experimental data for all sodium halide salts [9, 10] the radius of Na^+ was adjusted to be 2.5 Å.

We will proceed in a similar way in the present Monte Carlo study. The hydrated radius of Na^+ will be adjusted to fit the experimental data for the surface tension of the NaCl electrolyte–air interface. We find that a good fit of experimental data can be obtained if $a_{Na} = 1.8$ Å, see figure 4. The change of the hydration radius of Na^+ is the result of electrostatic and hard-core correlations neglected within the Poisson–Boltzmann theory. Curiously the new value of the hydrated radius of Na^+ is exactly the Latimer radius of this ion. The Latimer radii are obtained by fitting the experimental hydration free energies to the Born model of solvation [28]. This suggest that the Latimer radii of other cations might also be able to account for the surface tensions of their respective alkali metal salts such as, for example, CsCl, KCl, NaCl and LiCl. The Latimer radii for Cs^+, K^+ and Li^+ are 2.54, 2.18 and 1.45 Å, respectively [28]. Using these radii in our simulations, we obtain the surface tensions of the respective alkali metal salts. The calculated surface tensions are plotted in figure 4, where they are also compared to the experimental data [29, 30]. As can be seen, the agreement between theory and experiment is very reasonable. We next calculate the surface tensions for other kosmotropic sodium salts: fluoride, iodate and bromate, using the same methodology. The hydrated radii of F^-, IO_3^- and BrO_3^- are 3.52, 3.74 and 2.41 Å, respectively [9–11]. Note that, while, F^- and IO_3^- remain fully hydrated at the interface, BrO_3^- is very weakly hydrated, similar to Cl^- ion. The calculated surface tensions for NaF, $NaIO_3$ and $NaBrO_3$ are compared with the experimental data in figure 5, again showing a reasonable agreement.

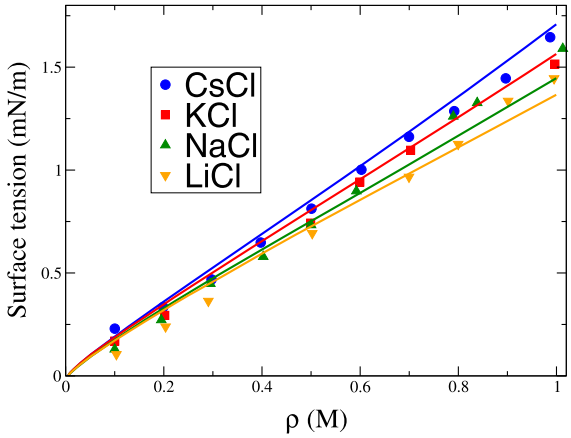

Figure 4. Surface tensions for cesium, potassium, sodium and lithium chloride. Solid lines are our simulation results and the symbols are the experimental data [29, 30].

4. Conclusions

We have presented a Monte Carlo simulation approach for calculating surface tensions of electrolyte solutions of kosmotropic (structure-making) ions. The underlying theory is based on the observation that kosmotropic ions remain hydrated near the air–water interface [9, 10]. Thus, they are not able to approach the Gibbs dividing surface closer than their hydration radii. The MC simulations confirm the earlier modified Poisson–Boltzmann theory, in particular showing that the correlational effects omitted by the PB equation can be captured by a suitable renormalization of the cationic radii. Within the modified Poisson–Boltzmann formalism it was necessary to use $a_{Na} = 2.5$ Å in order to account for the experimental data, while within the MC formalism this size was reduced to $a_{Na} = 1.8$ Å. Curiously the value 1.8 Å is precisely the Latimer radius of Na^+. This suggested, that the surface tensions of other alkali metal salts can also be calculated using the Latimer radii of their respective cations. This is exactly what was found when the results of simulations were compared with the experimental data. At the moment it is not clear why Latimer radii are relevant for the hydration of cations near the air–water interface. The hydration of anions, on the other hand, is completely correlated with the Jones–Dole viscosity B coefficient [34]—anions with positive

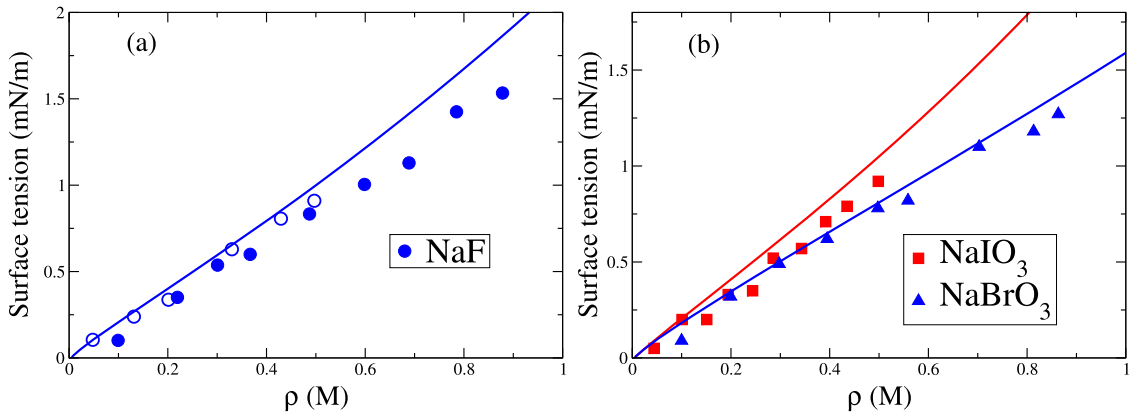

Figure 5. Surface tensions for (a) sodium fluoride, (b) iodate and bromate. Full circles represent the data of Matubayasi *et al* [31] and the open circles are the data of Weissenborn and Pugh [32]. Squares and triangles are the data of Matubayasi [33]. The solid lines are our simulation results.

B remain hydrated at the interface, while the ones with negative *B* lose their hydration sheath [10].

For now we have only used MC simulations to study surface tensions of salts with kosmotropic anions. Implementation of the present formalism for simulations of chaotropic ions is technically more challenging since it requires accounting for the non-trivial electrostatics as these ions cross the dielectric interface [8]. Work in this direction is now in progress.

Acknowledgments

This work was partially supported by the CNPq, Fapergs, INCT-FCx and by the US-AFOSR under grant FA9550-09-1-0283. We also thank the Centro de Fisica Computacional—IF/UFRGS for computer time.

References

[1] Debye P W and Hückel E 1923 *Phys. Z.* **24** 185
[2] Levin Y 2002 *Rep. Prog. Phys.* **65** 1577
[3] Langmuir I 1917 *J. Am. Chem. Soc.* **39** 1848
[4] Wagner C 1924 *Phys. Z.* **25** 474
[5] Onsager L and Samaras N N T 1934 *J. Chem. Phys.* **2** 528
[6] Boström M, Williams D R M and Ninham B W 2001 *Langmuir* **17** 4475
[7] Jungwirth P and Tobias D J 2006 *Chem. Rev.* **106** 1259
[8] Levin Y 2009 *Phys. Rev. Lett.* **102** 147803
[9] Levin Y, dos Santos A P and Diehl A 2009 *Phys. Rev. Lett.* **103** 257802
[10] dos Santos A P, Diehl A and Levin Y 2010 *Langmuir* **26** 10778
[11] dos Santos A P and Levin Y 2010 *J. Chem. Phys.* **133** 154107
[12] Markovich G, Pollack S, Giniger R and Cheshnovski O 1991 *J. Chem. Phys.* **95** 9416
[13] Garrett B 2004 *Science* **303** 1146
[14] Ghosal S, Hemminger J, Bluhm H, Mun B, Hebenstreit E L D, Ketteler G, Ogletree D F, Requejo F G and Salmeron M 2005 *Science* **307** 563
[15] Heydweiller A 1910 *Ann. Phys. (Lpz.)* **33** 145
[16] Hofmeister F 1888 *Arch. Exp. Pathol. Pharmakol.* **24** 247
[17] Knipping E M, Lakin M J, Foster K L, Jungwirth P, Tobias D J, Gerber R B, Dabdub D and Finlayson-Pitts B J 2000 *Science* **288** 301
[18] dos Santos A P and Levin Y 2011 *Phys. Rev. Lett.* **106** 167801
[19] Ho C H, Tsao H K and Sheng Y J 2003 *J. Chem. Phys.* **119** 2369
[20] Jackson J D 1999 *Classical Electrodynamics* (New York: Wiley)
[21] Messina R 2002 *J. Chem. Phys.* **117** 11062
[22] Lindell I V 1992 *Radio Sci.* **27** 1
[23] Norris W T 1995 *IEE Proc., Sci. Meas. Technol.* **142** 142
[24] dos Santos A P, Bakhshandeh A and Levin Y 2011 *J. Chem. Phys.* **135** 044124
[25] Bakhshandeh A, dos Santos A P and Levin Y 2011 *Phys. Rev. Lett.* **107** 107801
[26] Allen M P and Tildesley D J 1987 *Computer Simulations of Liquids* (Oxford: Oxford University Press)
[27] Panagiotopoulos A Z and Kumar S 1999 *Phys. Rev. Lett.* **83** 2981
[28] Latimer W M, Pitzer K S and Slansky C M 1939 *J. Chem. Phys.* **7** 108
[29] Matubayasi N, Yamamoto K, Yamaguchi S, Matsuo H and Ikeda N 1999 *J. Colloid Interface Sci.* **214** 101
[30] Matubayasi N, Matsuo H, Yamamoto K, Yamaguchi S and Matuzawa A 1999 *J. Colloid Interface Sci.* **209** 398
[31] Matubayasi N, Tsunemoto K, Sato I, Akizuki R, Morishita T, Matuzawa A and Natsukari Y 2001 *J. Colloid Interface Sci.* **243** 444
[32] Weissenborn P K and Pugh R J 1996 *J. Colloid Interface Sci.* **184** 550
[33] Matubayasi N 2012 unpublished
[34] Jenkins H D B and Marcus Y 1995 *Chem. Rev.* **95** 2695